THE JOURNAL OF PHYSICAL CHEMISTRY C

Article

pubs.acs.org/JPCC

Molecular Dynamics Simulations of Water Confined in Calcite Slit Pores: An NMR Spin Relaxation and Hydrogen Bond Analysis

Sylvia M. Mutisya,[†] Alexsandro Kirch,[‡] James M. de Almeida,[†] Verónica M. Sánchez,[†,§] and Caetano R. Miranda*[,‡]

[†]Centro de Ciências Naturais e Humanas, Universidade Federal do ABC, Santo André, São Paulo, Brazil

[‡]Instituto de Física, Universidade de São Paulo, CP 66318, 05315-970, São Paulo, São Paulo, Brazil

ABSTRACT: We study water confined in calcite (104) slit pores from 6 to 1 nm by molecular dynamics. By determining NMR parameters combined with hydrogen bond network analysis, we provide an important contribution to the understanding of the dynamics of water confined. The water dynamics was found uncorrelated upon confinement within calcite, with the translational dynamics highly dependent on the local density variations and the rotational dynamics varying with local hydrogen bond connectivity. A water layered structuring is observed, and the layer by layer analysis reveals that translational dynamics are the main contribution to spin relaxation of near surface water molecules. The T_2 relaxation time for water molecules directly hydrogen bonded to the surface is short and pore size independent; however, a bulk-like spin relaxation is observed at the center of pores larger than 3 nm. The hydrogen bond network of confined water has a more continuous path topology that results in the slightly longer rotational correlation time for water located up to 2 nm from the surface. Moreover, the number of tetrahedral geometric patterns which are associated with bulk water is reduced upon confinement. The confinement effects are enhanced mainly in the 1 nm pore due to overlap of surface effects.

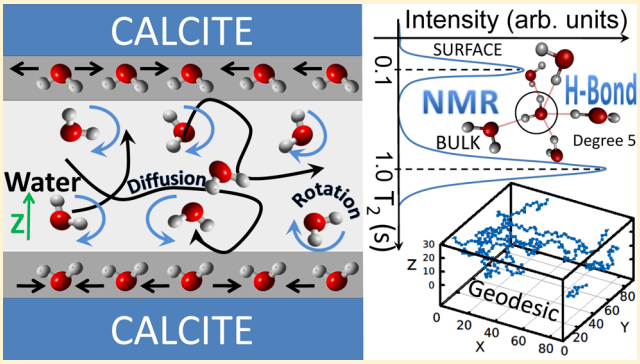

1. INTRODUCTION

Calcite, an anhydrous calcium carbonate polymorph, is a major component of carbonate reservoir rocks. Its interaction with fluids is important in geological processes[1] such as biomineralization,[2] CO_2 sequestration,[3] and oil exploration and production.[4] To control these processes, it is necessary to consider the porous nature of carbonate rocks, which can modify the fluid−rock interaction due to the spatial fluid confinement, and variations on the chemical and electrostatic environment. However, the heterogeneous pore distribution, pore type, pore connectivity, and grain size[5−8] in carbonates pose challenges in the determination of the properties of interest.[9,10] Many studies have focused on understanding the carbonate/fluid interactions[11−15] which influence the properties of the confined fluids. However, many aspects of the structure, dynamics, and energetics of fluid/carbonate interaction are still incompletely understood, and this remains a topic of active research.

Among the carbonate minerals, calcium carbonate ($CaCO_3$) is one of the most abundant minerals on Earth. Many studies has been focused on the calcite (104) surface, which is the most stable one.[16−18] In this line, several works have addressed the water/calcite (104) surface interface both experimentally[17,19−27] and theoretically.[26,28−37] Within the experimental works, X-ray scattering[21,24] and X-ray reflectivity techniques were employed to determine calcite surface speciation[22] as well as to obtain calcite/water interface structure.[23] Fenter and Sturchio[21] showed two distinguishable water density layers with the peaks observed at (2.14 ± 0.02) Å and (3.44 ± 0.12) Å.

First-principles simulations show an associative molecular adsorption type for the first water layer on a crystalline surface.[31,33,36,38,39] In addition, molecular dynamics studies reported that water exhibits two structured layers in the vicinity of a calcite surface (104), with a third layer being weakly ordered.[23,29]

The effect of calcite on water dynamics has been extensively investigated by calculating the translational diffusion,[20,32,40] residence times,[32,41,42] and the water exchange rates.[40] The overall slowdown is attributed to the structuring of water due to its interaction with the surface. However, a detailed analysis of the hydrogen bond network of water confined in calcite slit pores which may have strong effect on these properties is still missing.

Molecular dynamics simulations by Kerisit and Parker[32] showed that water diffusion is anisotropic near the calcite surface. The calculated parallel diffusion coefficients in the first and second layers are 0.6×10^{-9} m^2/s and 0.9×10^{-9} m^2/s respectively, while the diffusion in the normal direction was

Received: December 9, 2016
Revised: March 10, 2017
Published: March 13, 2017

DOI: 10.1021/acs.jpcc.6b12412
J. Phys. Chem. C 2017, 121, 6674−6684

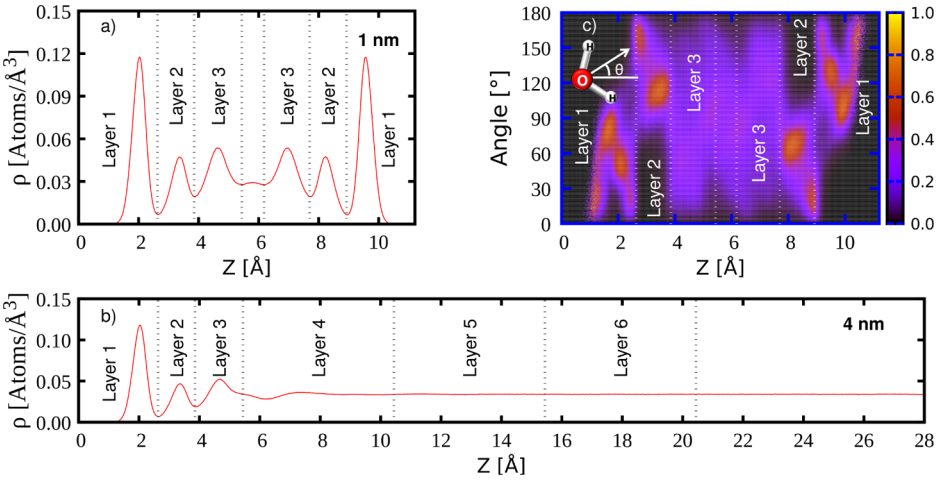

Figure 1. (a) Fluctuations in oxygen atom density profile along the z axis perpendicular to the surface. The location of the calcite surface ($z = 0$) was defined from the mean surface calcium atom positions. Three layers can be identified with valleys at positions 2.67 Å, 3.89 Å, and 5.48 Å with respect to the calcite wall. (b) Probability distribution of water dipole moment orientation along the z direction for 1 nm calcite pore. Angle 90° is parallel, 0° is pointing away, and 180° is oriented toward the surface. (c) Density profile of a 4 nm slit pore illustrating layer 1−6 definition.

$<0.2 \times 10^{-9}$ m^2/s in the first two layers. In this study, the diffusion at the center of the pore was twice the bulk water diffusion which was attributed to low density, in contrast to simulations by Perry et al.[40] which indicate that the diffusion at the center of the pore is bulk-like. Anisotropic parallel diffusion was observed for other fluids (methane, nitrogen, and carbon dioxide) confined in calcite pores.[43]

Surface exchange of water molecules confined in calcite pores is observed by molecular dynamics simulation to occur at a rate of one exchange per 10 ps.[40] In addition, the residence time of water in the first layer is calculated to be about 6 times greater than that of the second layer,[32] despite having comparable structural and dynamical properties. A recent study of structure and dynamics of water at step edges of the $\{10\bar{1}4\}$ surface[41] associated the wide range of residence times with two types of water near the surface, with the shorter residence times reflecting the unbound water molecules.

From previous studies on calcite/water interactions, density oscillations of water attributed to excluded volume effect[44,45] extend about 5 Å from the surface. However, the nonuniform O atom density profile spacing indicates that other factors are involved in the water layering near the calcite surface.[45] Over the years, nuclear magnetic resonance (NMR) relaxation techniques have been used in the characterization[9,46−50] of confined fluid dynamics in carbonates. However, experimental investigations of water dynamics confined in calcite pores do not provide distinct information about the surface and center of pore water molecules as well as the individual contribution of rotation and translational dynamics to the overall spin relaxation.

In this work, by using molecular dynamics simulations, we aim to provide additional atomistically detailed analysis of the effects of surface and confinement to water inside calcite slit pores (and hydrophilic slit pores in general) using a new approach that combines theoretical NMR property calculations and hydrogen bond analysis based on graph theory.[51] Our results show the contribution of rotational and translational dynamics to the NMR relaxation time T_2 in confinement. Detailed description of the dynamics and hydrogen bond network structure of water in each layer is given in order to understand the changes in the properties as the water molecules transition from the bulk region to the surface. To address the effect of extreme confinement, we vary the pore sizes from 6 to 1 nm.

2. METHOD

We use classical molecular dynamics simulations to obtain a set of trajectories of water inside calcite slit pores in thermodynamic equilibrium. The properties analyzed from the trajectories include water density profiles, translational dynamics, reorientational dynamics, hydrogen bond connectivity, water average residence times, and the time persistence of hydrogen bonds. The molecular dynamics calculations are performed by using the large atomic/molecular massively parallel simulator (LAMMPS)[52] package.

The calcite structure was obtained from the crystallographic data published by Markgraf and Reeder.[53] It was cleaved to expose the (104) surface, due to its major stability.[16−18] The calcite slab was converged to nine layers, exposing mirror calcite surfaces (104) on each surface of the pore. The resulting cell dimensions were a = 96.9 Å, b = 88.8 Å, and c = 27.2 Å, with a total of 3888 $CaCO_3$ units. The PACKMOL[54] package was used to add water molecules randomly within the slit pores at a density of 1 g/cm^3.

We adopt the interatomic potential derived from Raiteri et al.[29,35] works. In this model, the carbonate ion is flexible as well as the water model SPC/Fw[55] employed, giving a better description of the water/calcite interface.[22] These flexible models improve the description of confined systems, as the bond lengths and angles can be altered in such an environment. The non bonded pair interactions are truncated at a cutoff distance of 9 Å. The long-range electrostatic interactions are solved by the PPPM[56] method with a precision of 10^{-5} on the forces. All simulations were carried out with periodic boundary conditions in all the directions.

Conjugate gradient algorithm was used to minimize the forces and energy. The equilibration procedure involved first adding a Gaussian velocity distribution of 10 K (with no net linear or angular momentum) and running a 50 ps simulation in NVE ensemble and a time step of 1 fs. Next the time step is reduced to 0.5 fs, and a 500 ps simulation was performed in NVT ensemble at 400 K. The increase of the temperature was

DOI: 10.1021/acs.jpcc.6b12412
J. Phys. Chem. C 2017, 121, 6674−6684

to avoid any local minima due to a possible artificial liquid structuring from the initial configuration. Then a 250 ps simulation in NVE ensemble was followed by a 1 ns NPT simulation at 300 K and 1 atm. The production runs were performed for 1 ns in NVT ensemble. A longer production run of 5 ns was performed for the analysis of the residence times and rotational dynamics. For the NVT simulations we have employed a Nosé–Hoover thermostat,[57,58] and for the NPT simulations a Nosé–Hoover barostat[59] was added.

3. RESULTS

3.1. The Water Density Profile at Calcite Interface. The water density profile along the confinement direction of the slit pores shows an oscillation as shown in Figure 1a for a 1 nm pore. In all the pore sizes, there is formation of three distinct peaks in the vicinity of the surface in agreement with other works on water–calcite interfaces.[23,32,60] Beyond the three layers, there is a mild oscillation up to 8 Å for 2–6 nm pores, exhibiting a constant bulk water density beyond this point (see Figure 1b for a 4 nm pore). For the 1 nm pore, the effect of confinement is enhanced since no constant density was observed at the center of the pore, with water molecules forming six structured layers. The superposition of surface effects of both surfaces of the slit leads to this atypical behavior.

Ordering of water near the calcite surface was investigated by calculation of the orientation of the dipole moment vector (Figure 1c), where water dipole vectors form an angle θ with respect to the surface normal. It can be observed that, for each structured layer, the water dipole is oriented differently. In layer 1, there are two preferential dipole moment orientations: parallel to the surface ($\theta \approx 90°$) and pointing away from the calcite surface ($\theta \approx 50°$). Other studies interpreted both orientations to lead to weak hydrogen bonds between water molecules and the surface carbonate groups.[29,32,61] Water molecules in layer 2 are oriented preferably toward the calcite surface as indicated by an angle $\theta > 90°$. This orientation is expected to result in strong directional hydrogen bonds with the surface carbonate groups.[40] Even though there is definite structuring of water in the vicinity of the calcite surface, we did not observe any curvature on the surface due to its interaction with water, despite the use of a flexible model for the carbonate groups. This is presumably because of the high stability of the (10.4) surface and stabilization of the carbonate groups by hydrogen bonding with the surface water molecules. Detailed analysis of the water/surface hydrogen bond connectivity will be presented in subsequent sections. In layer 3, the dipole vector orientations are not well-defined, indicating less arrangement, in line with previous results on calcite/water interface.[20,27] Beyond layer 3, more precisely after 8 Å, the orientation of the dipole vector has a bulk-like behavior.

3.2. Translational Dynamics. The translational dynamics of water are quantified by calculating the self-diffusion coefficient D from the slope of the mean square displacement (MSD) as a function of time according to Einstein's relation:[62]

$$D = \lim_{t\to\infty} \frac{\langle |\mathbf{r}(t) - \mathbf{r}(0)|^2 \rangle}{6t} \quad (1)$$

where $\mathbf{r}(t)$ is the position vector of the water molecule center of mass at time t. The angular brackets denote an average over time origins and all water molecules. The diffusive behavior of the water confined in the calcite slit pores was investigated by plotting on a log–log scale the MSD data versus the simulation time. From these, the normal diffusive linear dependence in t was observed starting from 10 and 100 ps for 3–6 nm and 1–2 nm pores, respectively. As shown in Figure 2 a, D increases with

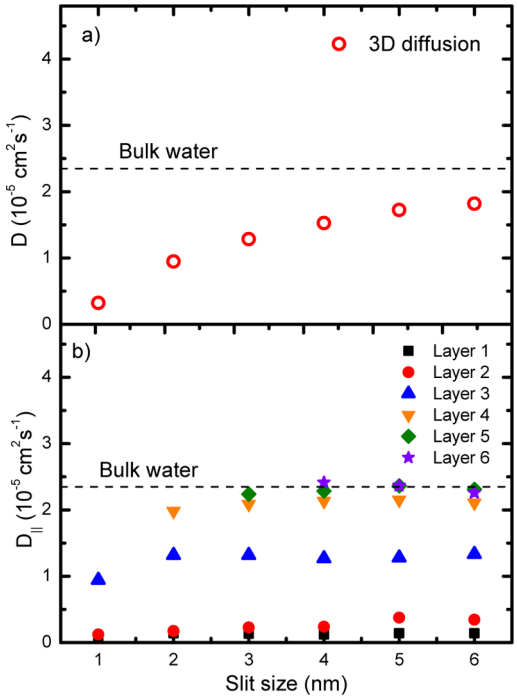

Figure 2. (a) 3D self-diffusion coefficient of water inside calcite slit pores as a function of pore size. (b) Parallel 2D self-diffusion coefficient as a function of distance from the calcite surface and pore size. Error bars from the fitting of the MSD data are smaller than the symbol sizes.

increase in the pore size, approaching the bulk water value for larger pores. The simulated bulk water self-diffusion coefficient in this work is 2.35×10^{-5} cm^2 s^{-1} in agreement with an experimental value of 2.3×10^{-5} cm^2 s^{-1}.[63] Even for the largest pore investigated in work (i.e., 6 nm pore), the self-diffusion is considerably smaller than the bulk diffusion despite having a bulk density profile at the center of the pore. The slowdown of the overall translational dynamics upon confinement is attributed to the strong interaction between water molecules and the calcite surface, which leads to slower mobility of the surface water molecules. The hindered mobility of water molecules confined in calcite surfaces has been observed in other studies.[20,32,40]

To quantify the magnitude of the calcite/water interactions to water diffusion, analysis was performed for water in different regions within the pore. Based on the density profile results, the calcite slit pores were subdivided into 6 regions, which consisted of the three layers near the surface, herein termed layer 1, layer 2, and layer 3, with layer 1 being nearest to the surface, and three more slabs each of 5 Å, termed layer 4, layer 5, and layer 6 (see Figure 1b). Due to hindered mobility in the z direction,[20] only parallel diffusion was calculated according to the methodology developed by Liu et al.[64] Using this approach the parallel self-diffusion coefficient $D_{\parallel}(\{z\})$ is obtained by the modified Einstein equation:

$$D_{\parallel}(\{z\}) = \lim_{t\to\infty} \frac{\langle \Delta\mathbf{r}(t)^2 \rangle_{\{z\}}}{4P(t)t} \quad (2)$$

DOI: 10.1021/acs.jpcc.6b12412
J. Phys. Chem. C 2017, 121, 6674–6684

where $\{z\}$ represents the set of molecules that remain in the slab centered at a distance z from the surfaces during the interval $[0, t]$. $P(t)$ is the survival probability function which relates the number of molecules $N(t)$ that remain in the slab in the time interval $[0,t]$ to the number of molecules $N(0)$ that were present at the initial time $t = 0$, averaged over all time steps T.

$$P(t) = \frac{1}{T}\sum_{t=1}^{T}\frac{N(t)}{N(0)} \tag{3}$$

To obtain the self-diffusion coefficient for water in layer 1, layer 2, and layer 3, the MSD/$P(t)$ data was fitted from 2 to 8 ps, where the curve was linear. Due to the small size of the first three layers, i.e., layer 1 = 2.62 Å, layer 2 = 1.26 Å, and layer 3 = 1.54 Å, water molecules leave the specified layers within short times; thus the statistical accuracy on the MSD/$P(t)$ data becomes rather poor after a few picoseconds. For water molecules beyond layer 3, the MSD was linear throughout the simulation time.

In comparison to bulk water, the diffusion coefficient of water in layer 1 is reduced by 96% in 1 nm pore and by ≈94% for 2−6 nm pores, while in layer 2 it is reduced by 94% in the 1 nm pore with this value reducing to 85% in the 6 nm pore (see Figure 2 b). The range of values obtained is in agreement with simulations by Rahaman et al.[20] at 75% and 50% relative humidities, where at these lower relative humidities the calcite surface is covered by water molecules located in the first and second water layers.

The slowdown of the dynamics in layer 1 and layer 2 is attributed to the strong calcite/water interactions. As we move away from the surface, the water diffusion increases considerably, as can be seen for water in layer 3, despite the density being high in this region. Correlation between these findings with other properties will be given in Discussion.

From the density profiles, the water density reaches bulk water value at around 8 Å from the surface. In relation to diffusion, our findings indicate that the water diffusion is lower than the bulk value whenever there is a slight perturbation in the density profile. In our systems, this corresponds to water molecules located up to layer 4 (see Figure 2 b). The translational dynamics are bulk-like at ≈15 Å from the surface, as shown for water in layer 5. This implies that the water located at the center of 1 and 2 nm pores is diffusing more slowly than bulk water.

3.3. Rotational Dynamics. The rotational dynamics are analyzed by computing the second order reorientation time−correlation function $C_2(t)$, for the water HH-bond vector $\mathbf{u}$, which is given by

$$C_2(t) = \langle P_2[\mathbf{u}(0)\cdot\mathbf{u}(t)]\rangle \tag{4}$$

where P_2 is the second order Legendre polynomial.[65] The relaxation time can be compared with that measured in ^{1}H NMR experiments for a rotation about the HH vector.[66] To obtain the rotational correlation time τ_c, the data was fitted to a stretched exponential function $a_0\, e^{-(t/\tau_c)^{\beta}}$ which has been used previously to fit correlation functions for supercooled water.[67]

The rotational correlation time for all the water confined in the calcite pores decreases with increase in pore size as shown in Figure 3 a. Water reorientation is reduced by a factor of ≈4 for the 1 nm pore, with this value decreasing as the pore sizes are increased. Similar studies obtained a reduction in water reorientation by a factor of 2−3 for water confined in zeolites.[68]

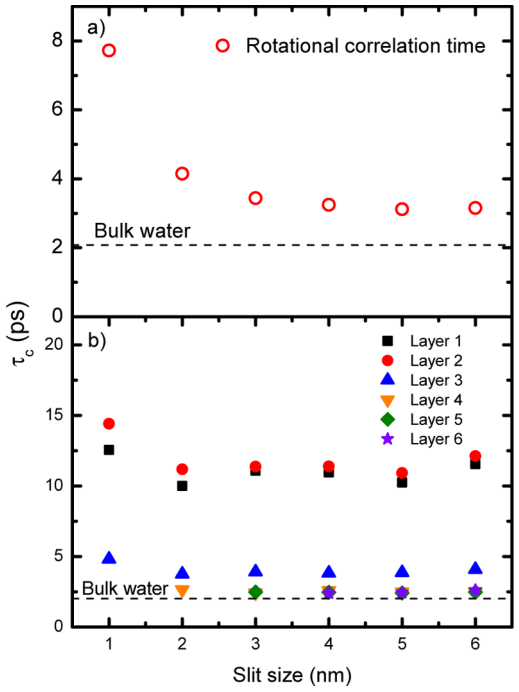

Figure 3. (a) Rotational correlation time for all the water inside calcite slit pores. (b) Rotational correlation time as a function of distance from the surface. Error bars from the exponential fitting are roughly the same size as the symbols.

Analysis of the rotational dynamics as a function of distance from the calcite surface is done by using a modified equation for the reorientation time−correlation function[69] averaged over only the water molecules which remain in the selected slab for the entire time t (see section 3.6).

$$C_2(t)_{\{z\}} = \frac{1}{P(t)}\langle P_2[\mathbf{u}(0)\cdot\mathbf{u}(t)]\rangle_{\{z\}} \tag{5}$$

$P(t)$ is the survival function (eq 3), and $\{z\}$ represents the set of molecules that remain in the slab centered at a distance z from the surfaces during the interval $[0,t]$.

Layer by layer analysis indicates that water in layer 2 has the longest rotational correlation time (Figure 3 b) despite its position further from the calcite surface than layer 1. Previous studies[40] related the enhanced stability of water molecules in layer 2 to its double coordination with the surface. Further analysis of the hydrogen bonding in this layer which may result to this anomalous behavior is presented in Discussion. Similar to the self-diffusion coefficient, the rotational correlation time increases considerably in layer 3. However, in contrast to diffusion, the rotation of water molecules beyond layer 3 has a constant value of ≈2.4 ps in all pores, which is slightly higher than the calculated bulk water value of 2.1 ps. Our simulated reference rotational correlation time for bulk water is in agreement with the experimental value of 2.0 ps.[70] The longer rotational correlation time at the center of the pore is attributed to the slight strengthening of water−water hydrogen bonds[68] upon confinement.

These findings indicate that the translational and rotational dynamics of water inside the calcite slit pores are uncorrelated, showing that $D_{\parallel}(\{z\})$ increases with a slower rate than τ_c. Similar results were obtained for computational studies of water confined in two β cristobalite plates.[69]

DOI: 10.1021/acs.jpcc.6b12412
J. Phys. Chem. C 2017, 121, 6674−6684

Thus far, it has been shown that the dynamical properties of water confined in calcite slit pores depend on calcite surface water interactions, with the behavior at the center of the pores dependent on the size of the pores. Effects of extreme confinement are observed in the 1 and 2 nm pores for translational dynamics, and for only 1 nm pore for the rotational dynamics, illustrating the translational−rotational decoupling. We use this information to calculate the NMR T_2 relaxation time described in the next section.

3.4. T_2 NMR Relaxation Time. The determination of T_2 relaxation time of proton bearing fluids is a widely accessible experimental technique used to study the properties of porous media. However, although the NMR signal contains the contribution of all relaxing spins, it is difficult to disentangle the contributions of water in different regions of the pore and the main mechanisms leading to the relaxation. By simulating the relaxation rates in each layer, we aim to provide local variation of the spin relaxation times, which is helpful in enhancing the interpretation of the experimental NMR signal response obtained from the contribution of all molecules.

The fundamental theory for spin relaxation was developed by Bloembergen, Purcell, and Pound (BPP).[71] According to BPP theory, the T_2 relaxations of hydrogen proton bearing fluids are facilitated by dynamic fluctuations in the local magnetic fields arising from intra- and internuclear magnetic dipole−dipole interactions. If the rotational and translational dynamics of dipolar couplings can be assumed to be stochastically independent of each other, the effective T_2 relaxation rates can be expressed as

$$\Gamma_2 \equiv \frac{1}{T_2} \approx \frac{1}{T_2^{\mathrm{rot}}} + \frac{1}{T_2^{\mathrm{trans}}} \tag{6}$$

where T_2^{rot} and T_2^{trans} correspond to rotation and diffusion of spins, respectively.

A rotating water molecule causes an intramolecular magnetic dipole−dipole interaction between the protons in a molecule, which is a function of the distance r separating the two spins. For the systems studied in this work, the characteristic time of decay τ_c of the correlation functions $C_2(t)$ and $C_2(t)_{\{z\}}$ is of the order of picoseconds, which satisfies the condition that $\omega^2\tau_c^2 \ll 1$, where ω is the Larmor frequency and τ_c is the rotational correlation time. The relaxation time rate is a function of the rotational correlation time and is given by[72]

$$\Gamma_2^{\mathrm{rot}} \equiv \frac{1}{T_2^{\mathrm{rot}}} \approx \left(\frac{\mu_0}{4\pi}\right)^2 \frac{3}{2}\frac{\gamma^4\hbar^2\tau_c}{r^6} \tag{7}$$

where γ is the gyromagnetic ratio, μ_0 is the permeability of free space, $\hbar$ is Planck's constant, and r is the separation of spins.

In addition, diffusing water molecules cause intermolecular magnetic dipole−dipole interactions. The T_2 relaxation time rate due to diffusing spins is as follows:[72]

$$\Gamma_2^{\mathrm{trans}} \equiv \frac{1}{T_2^{\mathrm{trans}}} \approx \frac{\pi}{5}\frac{N_s\gamma^4\hbar^2}{aD} \tag{8}$$

where N_s is the density of spins per cm^3, a is the distance of closest approach, and D is the translational self-diffusion coefficient.

The relaxation mechanisms at the solid/liquid interface are manifold. To understand the origin of NMR relaxation in different regions of the pore, we have investigated the relative contributions of rotational and translational dynamics. As shown in Figure 4 a, translational dynamics are the main

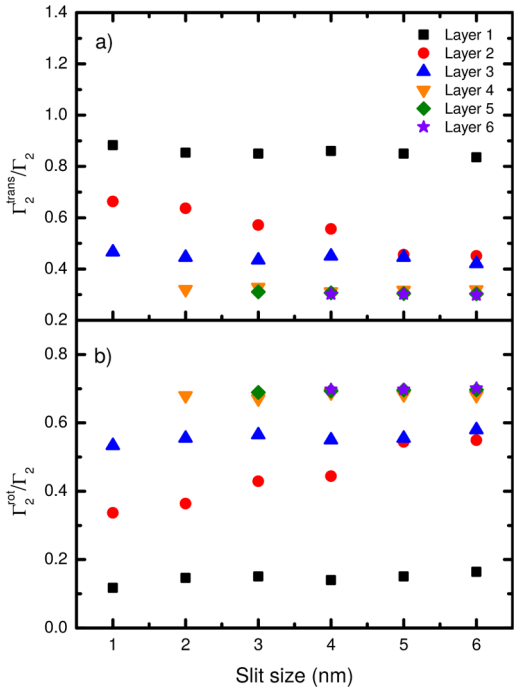

Figure 4. Relative contribution of (a) rotational and (b) translational dynamics to T_2 relaxation rates. The propagated errors are too small to represent in this graph.

contribution to the relaxation of spins in layer 1 indicated by the high $\Gamma_2^{\mathrm{trans}}/\Gamma_2$ ratio. These findings are associated with the local ordering of the water molecules in this layer resulting in inefficiency of water reorientation for the relaxation of magnetization through the fluctuations of intramolecular dipolar couplings.[73] The high density of water molecules in this region also promotes intermolecular interactions, further increasing the translational relaxation rate. In layer 2, intermolecular interactions dominate for pores 1−4 nm, with rotational dynamics dominating for 5−6 nm pores. Although the rotational correlation time is long in this region, there is an increase in self-diffusion coefficient (see Figure 2 b), thus leading to lower translational relaxation rates. In layer 3, the intramolecular and intermolecular interactions contribute almost equally to the total relaxation in all the pores studied in this work. On confinement, at the surface, it is expected that the intermolecular term might be partially suppressed with some rotational degrees of freedom entirely eliminated.[74] However, at the transition from the surface to the bulk, the details of the water dynamics at this scale are not well established; thus this knowledge is helpful in understanding the NMR spin relaxation of water under confinement. Beyond layer 3, intramolecular contribution to spin relaxation is 70% (Figure 4 b), which is in agreement with molecular dynamics simulations for bulk water.[75]

Based on the diffusion and rotation results, the surface layer was defined which consisted of layer 1 and layer 2 water molecules, and the rest of the water termed as bulk due to its bulk-like behavior. T_2 relaxation time was calculated for water located on the surface and in the bulk region.

In the bulk, fluids lacking additional means of interaction reveal long proton relaxation times, and from our simulations, the T_2 relaxation time for bulk water is 4.59 s, in agreement with an experimental value of 3.8 s[76] at 300 K. In confinement, relaxation is controlled by the surface/water interactions, and

DOI: 10.1021/acs.jpcc.6b12412
J. Phys. Chem. C 2017, 121, 6674−6684

the limitation in mobility is expected to reduce T_2. At the surface, the relaxation time is of the order of 10^{-1} s (Figure 5 a), in agreement with MD simulations for clays.[77] The values are irrespective of the pore size, implying that the relaxation of water near the calcite surface is governed by the surface interactions. However, for water in the bulk region, the relaxation time increases with increase in pore size, approaching the bulk water value for 4−6 nm pores.

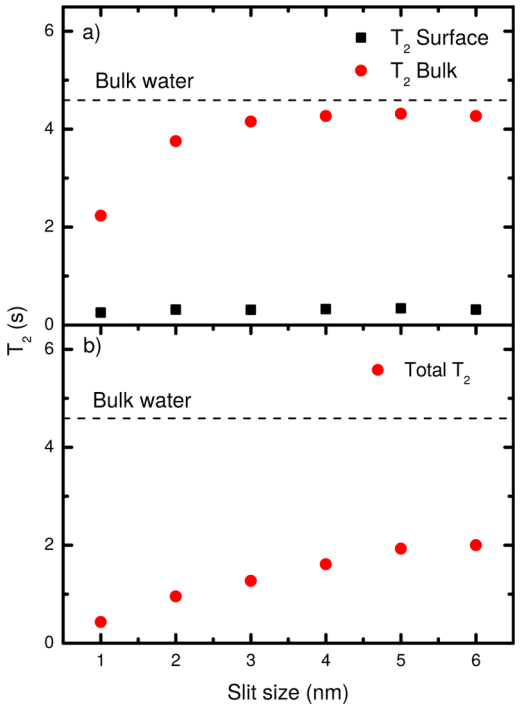

Figure 5. (a) T_2 relaxation time of water on the surface and bulk region of calcite 1−6 nm pores. (b) Total T_2 relaxation time as a function of pore size. The propagated errors are too small to be represented in this graph.

The total T_2 relaxation time in each pore obtained from both the surface and bulk contributions taking into account the surface to volume ratios[78,79] is presented in Figure 5 b). There is an overall reduction of the total T_2 relaxation time in the pores studied, with this value increasing as the sizes are increased. It is observed that the surface water interaction is the main contribution to the relaxation of spins, with only a small contribution coming from the bulk water. As the pores are increased, the surface to volume ratio decreases, which is expected to result in a significant contribution of bulk water to NMR T_2 relaxation rate eventually reaching the bulk water value. However, in this work, this limit was not established, due to high computational cost involved for large pores.

Although the interest here lies in the variation of the relaxation time of the spins due to confinement, the magnitude of the obtained values might be slightly overestimated[80,81] due to neglect of exchange of protons.

3.5. Hydrogen Bond Network Characterization. It is well established that the hydrogen bond network has tremendous effect on the properties of water.[82] Particularly for surface relaxation, the "bonding" of fluid molecules at the surface originates a faster relaxation rate of the protons, thus a shorter relaxation time compared with bulk water.[83] To provide more insight into the water/calcite interactions, a detailed analysis of the hydrogen bond network of confined water in calcite pores is presented in this section.

We obtain the hydrogen bond network structure of intermolecular interactions with the ChemNetworks code.[51] In this methodology, each water molecule is converted into a graph object. The graph edges are the hydrogen bonds that were determined by a geometric criterion: r_{O-H} is less than 2.5 Å, and simultaneously the O−H−O angle is greater than 150°.[84] With this definition we determined the average number of hydrogen bonds in bulk water as $\langle n_{HB} \rangle = 2.88$, which is less than the experimental value $\langle n_{HB} \rangle = 3.6$,[85] but remains within theoretically obtained values.[86,87] The information about bond connectivity has been assessed using geodesic analysis.

The water degree distribution (the number of hydrogen bonds) is determined according to the geometrical criterion described above. For water located in layer 1, we find that a water molecule forms preferentially 0 or 1 hydrogen bond with the other water molecules and 2 or 3 hydrogen bonds with the surface oxygens taken into account (see Figure 6a). This implies that water in this region forms almost entirely all its hydrogen bonds with the surface. Moving on to layer 2, we find that water is forming preferentially a total of 3 or 4 hydrogen bonds with the surface water interactions included and either 2 or 3 with the other water molecules. An interesting finding in this layer is that a substantial number of water molecules are

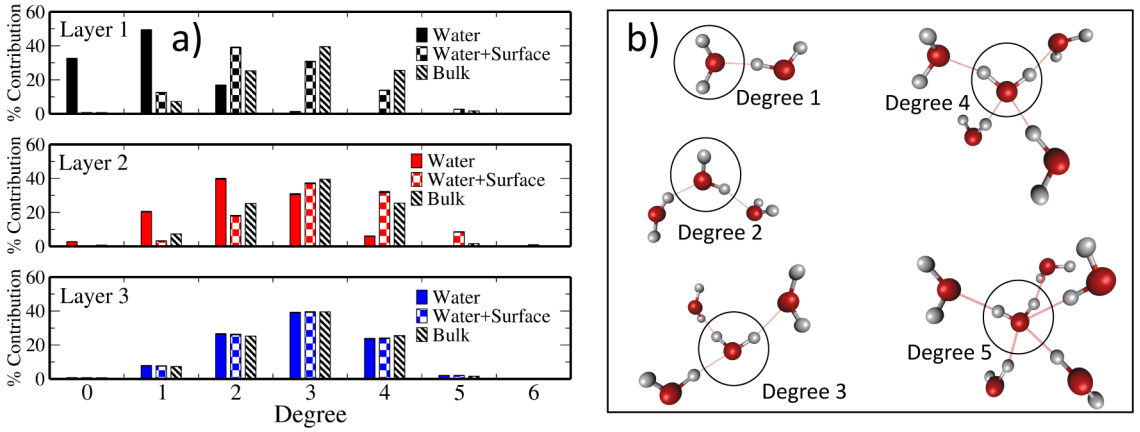

Figure 6. (a) Degree distribution of water and water + surface hydrogen bonds in each layer in comparison to bulk water. (b) Snapshots illustrating the hydrogen bond network for degrees 1, 2, 3, 4, and 5.

DOI: 10.1021/acs.jpcc.6b12412
J. Phys. Chem. C 2017, 121, 6674−6684

forming up to 5 hydrogen bonds (see Figure 6b for an illustration of degree 5 hydrogen bond network) in total (water + surface). From these results, it is clear that the average number of hydrogen bonds formed by water in this region is high, resulting in its stability, which we associate with the long rotational correlation time for water in this region. In layer 3, the water and water + surface contribution is equal, implying that all the hydrogen bonds are between water molecules. The degree distribution in this layer is equal to bulk water distribution meaning, that the surface does not interfere with the hydrogen bond network in this region.

Near the surface, the water molecules "prefer" to form hydrogen bonds with the surface atoms because it is energetically favorable. Thus, the number of water−water hydrogen bonds at the calcite interface is reduced in comparison to bulk water,[31] as shown by the reduced degree distribution in layer 1 and layer 2 regions. Other studies have shown that the strong interactions between the hydrophilic calcite surface and water impose the positions of the water on the interface.[20,29,33,40] As the pore size is increased, contributions to the degree distribution from the molecules near the calcite surface—layer 1 and layer 2—have reduced effect on the total system; thus it tends to bulk behavior.

A similar trend of degree distribution was also observed for the geodesic length (Figure 7a). Besides reducing the water−water degree in layer 1 and layer 2, the calcite surface also breaks the water network structure in shorter geodesics inside the layers with respect to the bulk water with the same layer width. This information has been assessed using geodesic analysis. Water molecules located in layer 3—which does not interact directly with the surface—has a geodesic distribution which is similar to that of bulk water.

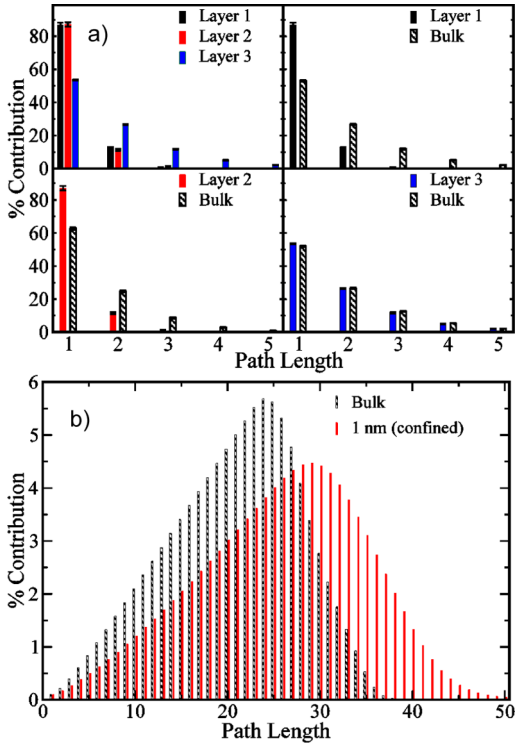

Figure 7. (a) Geodesic distribution in each layer compared with bulk water for equal slab width. (b) Geodesic distribution comparison between bulk water and water confined in a 1 nm calcite pore. Error bars represent standard error from the average. In panel b, the error bars are smaller than the line sizes.

Although on the surface the water hydrogen bonds are less structured, pore averaging shows a broader geodesic path distribution than for bulk water (Figure 7b). This indicates that confinement results in a much more structured system in suits of H-bonds, leading to connections that are extended for longer paths before breaking. Following the Ozkanlar et al.[88] interpretation, the broad distribution in confined systems with respect to bulk indicates that the surface promotes more contiguous bonded topology. As we increase the pore size from 2 to 6 nm, the path length distribution narrows down, approaching the bulk-like behavior for large pores.

We also searched for geometric patterns often found in systems that have hydrogen bonds. It is considered a geometric pattern, if the hydrogen bonds match the number of bonds and angles between atoms which form the structure.[51] To allocate a geometric pattern to a layer, we consider the patterns whose center of mass is inside the layer. Only water−water hydrogen bonds were taken into account. The search of geometric patterns allows investigation of the effects of confinement on the water network structure. This search revealed the main geometric patterns found in both the bulk and confined water. As seen in the Figure 8 a, the calcite surface has an effect on the geometric patterns formed in different regions of the pore. In layer 1 there is no formation of any geometric pattern. In layer 2 there are mainly cyclic tetramers. It is observed that larger structures (with higher number of water molecules) are not formed within this layer. Layer 3 has a distribution similar to that of bulk within the error bars.

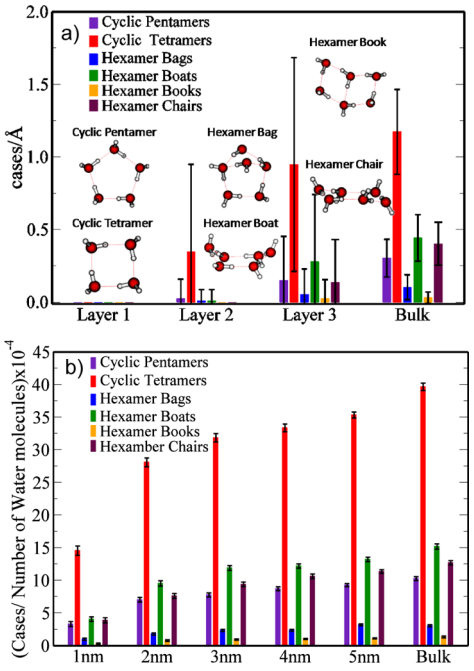

Figure 8. (a) Geometric pattern distribution within each layer for 1 nm water confinement. (The geometric pattern illustrations are adopted from ref 51.) Similar results were obtained for all the pores analyzed in this work. (b) Geometric pattern distribution in each pore in comparison to bulk water. The 6 nm pore system was not investigated because of the computational cost, but a similar trend is expected. Error bars represent standard errors.

DOI: 10.1021/acs.jpcc.6b12412
J. Phys. Chem. C 2017, 121, 6674−6684

In the 1 nm pore, the number of patterns is found to be reduced—relative to the bulk—due to calcite influence on the organization of water molecules throughout the whole system. For larger pores, we have more layers of water with bulk behavior, and we can observe the recovery of bulk-like patterns in the systems with increase in slit size (Figure 8 b).

3.6. Residence and Hydrogen Bond Persistence Time. The investigation of the residence time gives the details of the exchange of the water molecules with time. The survival probability function (see eq 3) data is fitted to an exponential function, $a_0\, e^{-(t/T_R)}$ to obtain the residence time T_R. Figure 9 a)

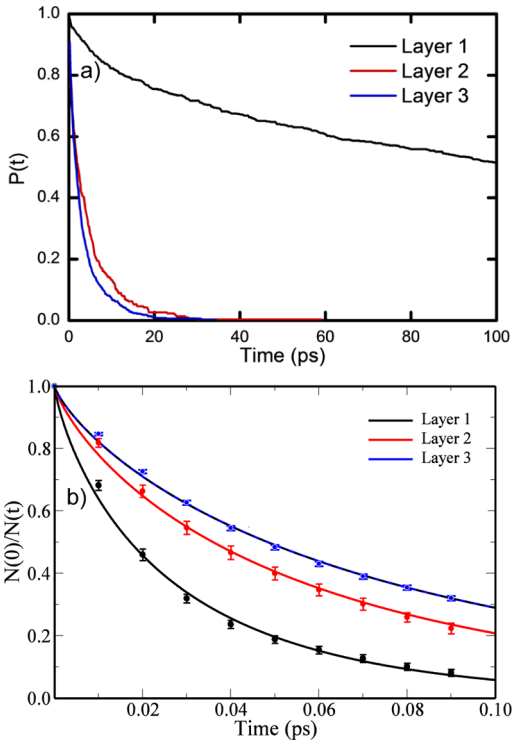

Figure 9. (a) Residence and (b) hydrogen bond persistence time for each layer in the 1 nm pore. Similar results are observed in all the pore sizes.

shows the survival probability functions of water located in layer 1, layer 2 and layer 3 of the 1 nm pore. For clarity only the first 100 ps are presented. $P(t)$ for the water molecules located in layer 2 and layer 3 decays at a high rate resulting in short residence times of 4.98 ± 0.03 ps and 3.11 ± 0.03 ps, respectively. These values are comparable to bulk water residence times T_R = 2−10 ps.[89] In contrast, the residence time for layer 1 water molecules is 214.59 ± 0.14 ps, which is similar to T_R for water adsorbed in an isolated Ca^{2+} ion.[41] Although water in layer 2 forms stable hydrogen bonds with the surface oxygen, it does not enter the hydration shell of the Ca^{2+} ions, hence the short residence times.

Hydrogen bonds break with time due to thermal vibrations. We calculate the time persistence of hydrogen bonds by considering only the molecules that remain in each layer for 0.1 ps. The time correlation function is calculated by considering the number of molecules $N(t)$ which are connected at time t in relation to the number of molecules $N(0)$ which were initially connected. The time correlation function for hydrogen bonds fits a stretched exponential decay in time $c(t) = \exp(-(t/t_p)^{\beta})$ which yields a persistence time $T_p = (t_p)^{\beta}$ with β = 0.8.

In Figure 9 b we show the hydrogen bond persistence correlation function of the first three layers in the 1 nm pore. It can be clearly seen that the hydrogen bond persistence time in layer 1 is shorter than in the subsequent layers due to the fast decay of the correlation function. From our fits we obtained hydrogen bond persistence times 0.06 ps, 0.10 ps, 0.13 ps, and 0.13 ps for water molecules in layer 1, layer 2, layer 3, and bulk water, respectively. The sub-picosecond time persistence is due to librations that are the primary source of hydrogen bond breaking.[84,90] The time persistence is directly related to the average number of hydrogen bonds, which must be broken, to obtain "mobile" water molecules. Therefore, the low degree distribution of the water−water hydrogen bonds leads to an increase in the librational frequency, hence the short hydrogen bond persistence time. So, layer 1 has weak hydrogen bonds. Similar results were obtained for water in contact with α-quartz surface by Ozkanlar et al.[88]

4. DISCUSSION

Using our approach of layer by layer analysis, we have presented the T_2 relaxation times in each layer, taking into account only the intermolecular and intramolecular interactions of water molecules which remain in a certain region during the entire simulation time. The decoupling of the translational and rotational dynamics results in an unpredictable local change of the NMR spin relaxation. Our results indicate that this cannot be explained solely by hydrogen bonding analysis. The slowdown of the water dynamics may be attributed to other factors including local high density, ionic interactions of the water with the surface atoms, and confinement. In this section, we discuss our findings in each layer and how confinement affects the properties investigated in this work.

The rotational correlation time τ_c of water molecules located in the surface layers is long in comparison to the bulk-like water (Figure 3b). From the investigations of the local hydrogen bonding in the surface layers, we showed that, in layer 1, water forms preferably a total of 2 or 3 hydrogen bonds while, in layer 2, it forms 3 or 4 bonds, with some water molecules forming up to 5 hydrogen bonds (Figure 6a). As a result, rotational correlation time is longer in layer 2 than in layer 1, which we attribute to the high average number of hydrogen bonds formed by water molecules in this region. The stability of water in layer 2 is also manifested in the formation of a very localized dipole vector orientation (see Figure 1c). Moving further to layer 3, we observe a significant decrease in the rotational correlation time, which we attribute to the bulk-like hydrogen bonding network in this region. The lower value in relation to bulk water is attributed to other factors such as high local density and confinement. The contribution of the intramolecular interactions to the T_2 relaxation time is mainly by water molecules located in layer 3 and beyond.

Similar to rotational dynamics, the parallel diffusion is slowest in layer 1 and layer 2. Although still slower than the bulk water diffusion, there is a significant increase in diffusion in layer 3. From our analysis, we showed that the hydrogen bonding connectivity is bulk-like in this region, thus we relate this slowdown in diffusion to the high local density. In the subsequent layers, we observe a slightly lower diffusion coefficient in layer 4, where the local density is perturbed. Intermolecular interactions are the main contribution to the T_2 relaxation time for water in layer 1 for all pores and in layer 2 for pores of size 1−4 nm.

DOI: 10.1021/acs.jpcc.6b12412
J. Phys. Chem. C 2017, 121, 6674−6684

The residence time, although not taken into account in our calculations for spin relaxation, is an important parameter to account for exchange of water from the surface to the bulk, and from this work we establish that it is highly dependent on the surface atom sites. The variation of the residence time is explained in terms of the association of water with the surface sites. Water located in layer 1 is coordinated to the Ca^{2+} ions, while layer 2 water is coordinated to the surface carbonate groups.[29,35] The short residence times of water in layer 2 are related to its location outside of the Ca^{2+} hydration shell.[41] The investigation of hydrogen bond persistence time, which is a measure of librational motions, indicates that we have shortest hydrogen bond persistence time in layer 1, with this value increasing as we move away from the surface. This implies that the water molecules on the surface form much weaker hydrogen bonds among themselves than in bulk water.

Confinement of water inside calcite pores alters the structure of water as indicated by the formation of a more contiguous hydrogen bond network (Figure 7b) and dipole moment vector arrangement (Figure 1c). This characteristic was evident on the slightly longer rotational correlation time than the bulk for water located up to 20 Å from the surface (Figure 3b). On confinement, the number of tetrahedral geometric patterns which are associated with bulk water is reduced (Figure 8b).

5. CONCLUSIONS

With the aid of molecular dynamics simulations, we have investigated the effects of calcite surface and extreme confinement on NMR spin relaxation parameters and hydrogen bond network structure. We have provided a detailed description of the properties of water confined in calcite slit pores as a function of the distance from the surface for pores of sizes 1−6 nm.

The main contribution to relaxation on the calcite surface is the intermolecular interactions, with intramolecular interactions dominating in layer 2 for 5−6 nm pores and all pores beyond layer 2. T_2 relaxation time on the calcite surface is of the order of 10^{-1} s for all the pores investigated. The total T_2 relaxation time calculated from both the surface and bulk contributions is highly dependent on the surface to volume ratio, and the main contribution is from the surface/water interactions. These findings are useful to the experimentalists seeking to analyze the measured NMR signals as well as act as a reference to theoreticians developing new theories to model spin relaxation in porous media.

Experimental analysis of fluids confined in nanopores predict a distorted hydrogen bonding network. In this work, we showed that confinement promotes formation of a more continuous hydrogen bond network in the whole pore but surface layer water molecules have a low degree distribution. Moreover, the search of geometric patterns indicated that there is a decrease of bulk-like patterns inside the pore, with no geometric patterns formed in layer 1. This detailed information cannot be accessed experimentally.

A strong effect of confinement is only evident when there is an overlap of surface effects from both sides of the pore. In our case, this is only observed in 1 nm pore for most of the properties investigated. The properties at the center of the pore are dependent on the pore size, and for the pores investigated in this work, spin relaxation is bulk-like for pores of at least 4 nm size.

AUTHOR INFORMATION

Corresponding Author

*E-mail: cmiranda@if.usp.br.

ORCID

Caetano R. Miranda: 0000-0002-8008-4907

Present Address

[§]V.M.S.: CSC, CONICET, Godoy Cruz 2390, 1425, Buenos Aires, Argentina.

Notes

The authors declare no competing financial interest.

ACKNOWLEDGMENTS

The authors acknowledge the financial support provided by PETROBRAS and the Brazilian funding agencies FAPESP, CNPq, and CAPES. The calculations have been performed at CENAPAD-SP, UFABC, and IFUSP supercomputer facilities. A special thanks to Dr. Paolo Raiteri for providing the LAMMPS routines necessary to perform the MD simulations using their force field and for the helpful discussions. We acknowledge the helpful discussions with Dr. Aurora Clark about ChemNetworks code.

REFERENCES

(1) Ahr, W. M. *Geology of carbonate reservoirs: the identification, description and characterization of hydrocarbon reservoirs in carbonate rocks*; John Wiley & Sons: 2011.

(2) Addadi, L.; Raz, S.; Weiner, S. Taking advantage of disorder: amorphous calcium carbonate and its roles in biomineralization. *Adv. Mater.* **2003**, *15*, 959−970.

(3) Huijgen, W. J. J.; Comans, R. N. J. *Carbon dioxide sequestration by mineral carbonation. Literature Review*; 2003.

(4) Lucia, F. J. *Carbonate reservoir characterization: an integrated approach*; Springer Science & Business Media: 2007.

(5) Enos, P.; Sawatsky, L. Pore networks in Holocene carbonate sediments. *J. Sediment. Res.* **1981**, DOI: 10.1306/212F7DF1-2B24-11D7-8648000102C1865D.

(6) Lucia, F. J. Petrophysical parameters estimated from visual descriptions of carbonate rocks: a field classification of carbonate pore space. *JPT, J. Pet. Technol.* **1983**, *35*, 629−637.

(7) Lucia, F. J. Rock-fabric/petrophysical classification of carbonate pore space for reservoir characterization. *AAPG Bull.* **1995**, *79*, 1275−1300.

(8) Anselmetti, F. S.; Eberli, G. P. Controls on sonic velocity in carbonates. *Pure Appl. Geophys.* **1993**, *141*, 287−323.

(9) Logan, W.; Horkowitz, J.; Laronga, R.; Cromwell, D. *Practical application of NMR logging in carbonate reservoirs*; SPE Annual Technical Conference and Exhibition; 1997.

(10) Akbar, M.; Petricola, M.; Watfa, M.; Badri, M.; Charara, M.; Boyd, A.; Cassell, B.; Nurmi, R.; Delhomme, J.-P.; Grace, M.; et al. Classic interpretation problems: evaluating carbonates. *Oilfield Rev.* **1995**, *7*, 38−57.

(11) Al Shalabi, E. W.; Sepehrnoori, K.; Delshad, M. Mechanisms behind low salinity water injection in carbonate reservoirs. *Fuel* **2014**, *121*, 11−19.

(12) Zeng, H.; Zou, F.; Horvath-Szabo, G.; Andersen, S. Effects of Brine Composition on the Adsorption of Benzoic Acid on Calcium Carbonate. *Energy Fuels* **2012**, *26*, 4321−4327.

(13) Austad, T.; Shariatpanahi, S.; Strand, S.; Black, C.; Webb, K. Conditions for a low-salinity enhanced oil recovery (EOR) effect in carbonate oil reservoirs. *Energy Fuels* **2012**, *26*, 569−575.

(14) de Lara, L. S.; Michelon, M. F.; Metin, C. O.; Nguyen, Q. P.; Miranda, C. R. Interface tension of silica hydroxylated nanoparticle with brine: A combined experimental and molecular dynamics study. *J. Chem. Phys.* **2012**, *136*, 164702.

DOI: 10.1021/acs.jpcc.6b12412
J. Phys. Chem. C 2017, 121, 6674−6684

(15) de Lara, L. S.; Michelon, M. F.; Miranda, C. R. Molecular dynamics studies of fluid/oil interfaces for improved oil recovery processes. *J. Phys. Chem. B* **2012**, *116*, 14667−14676.
(16) Skinner, A. J.; LaFemina, J. P.; Jansen, H. J. Structure and bonding of calcite; a theoretical study. *Am. Mineral.* **1994**, *79*, 205−214.
(17) Heberling, F.; Trainor, T. P.; Lützenkirchen, J.; Eng, P.; Denecke, M. A.; Bosbach, D. Structure and reactivity of the calcite-water interface. *J. Colloid Interface Sci.* **2011**, *354*, 843−857.
(18) MacInnis, I. N.; Brantley, S. L. The role of dislocations and surface morphology in calcite dissolution. *Geochim. Cosmochim. Acta* **1992**, *56*, 1113−1126.
(19) Rubasinghege, G.; Grassian, V. H. Role (s) of adsorbed water in the surface chemistry of environmental interfaces. *Chem. Commun.* **2013**, *49*, 3071−3094.
(20) Rahaman, A.; Grassian, V. H.; Margulis, C. J. Dynamics of water adsorption onto a calcite surface as a function of relative humidity. *J. Phys. Chem. C* **2008**, *112*, 2109−2115.
(21) Fenter, P.; Sturchio, N. Calcite (104)−water interface structure, revisited. *Geochim. Cosmochim. Acta* **2012**, *97*, 58−69.
(22) Fenter, P.; Geissbühler, P.; DiMasi, E.; Srajer, G.; Sorensen, L.; Sturchio, N. Surface speciation of calcite observed in situ by high-resolution X-ray reflectivity. *Geochim. Cosmochim. Acta* **2000**, *64*, 1221−1228.
(23) Fenter, P.; Kerisit, S.; Raiteri, P.; Gale, J. D. Is the calcite-water interface understood? Direct comparisons of molecular dynamics simulations with specular X-ray reflectivity data. *J. Phys. Chem. C* **2013**, *117*, 5028−5042.
(24) Geissbühler, P.; Fenter, P.; DiMasi, E.; Srajer, G.; Sorensen, L.; Sturchio, N. Three-dimensional structure of the calcite−water interface by surface X−ray scattering. *Surf. Sci.* **2004**, *573*, 191−203.
(25) Ricci, M.; Spijker, P.; Stellacci, F.; Molinari, J.-F.; Voïtchovsky, K. Direct visualization of single ions in the Stern layer of calcite. *Langmuir* **2013**, *29*, 2207−2216.
(26) Hamm, L. M.; Bourg, I. C.; Wallace, A. F.; Rotenberg, B. Molecular simulation of CO2-and CO3-brine-mineral systems. *Rev. Mineral. Geochem.* **2013**, *77*, 189−228.
(27) Marutschke, C.; Walters, D.; Cleveland, J.; Hermes, I.; Bechstein, R.; Kühnle, A. Three-dimensional hydration layer mapping on the (10.4) surface of calcite using amplitude modulation atomic force microscopy. *Nanotechnology* **2014**, *25*, 335703.
(28) Gale, J. D.; Raiteri, P.; van Duin, A. C. A reactive force field for aqueous-calcium carbonate systems. *Phys. Chem. Chem. Phys.* **2011**, *13*, 16666−16679.
(29) Raiteri, P.; Gale, J. D.; Quigley, D.; Rodger, P. M. Derivation of an accurate force-field for simulating the growth of calcium carbonate from aqueous solution: a new model for the calcite- water interface. *J. Phys. Chem. C* **2010**, *114*, 5997−6010.
(30) Demichelis, R.; Raiteri, P.; Gale, J. D.; Dovesi, R. Examining the accuracy of density functional theory for predicting the thermodynamics of water incorporation into minerals: The hydrates of calcium carbonate. *J. Phys. Chem. C* **2013**, *117*, 17814−17823.
(31) Wolthers, M.; Di Tommaso, D.; Du, Z.; De Leeuw, N. Calcite surface structure and reactivity: molecular dynamics simulations and macroscopic surface modelling of the calcite-water interface. *Phys. Chem. Chem. Phys.* **2012**, *14*, 15145−15157.
(32) Kerisit, S.; Parker, S. C. Free energy of adsorption of water and metal ions on the {1014} calcite surface. *J. Am. Chem. Soc.* **2004**, *126*, 10152−10161.
(33) Kerisit, S.; Parker, S. C.; Harding, J. H. Atomistic simulation of the dissociative adsorption of water on calcite surfaces. *J. Phys. Chem. B* **2003**, *107*, 7676−7682.
(34) Cooke, D. J.; Gray, R. J.; Sand, K. K.; Stipp, S. L. S.; Elliott, J. Interaction of ethanol and water with the {1014} surface of calcite. *Langmuir* **2010**, *26*, 14520−14529.
(35) Raiteri, P.; Gale, J. D. Water is the key to nonclassical nucleation of amorphous calcium carbonate. *J. Am. Chem. Soc.* **2010**, *132*, 17623−17634.
(36) Sanchez, V. M.; Miranda, C. R. Modeling acid oil component interactions with carbonate reservoirs: a first-principles view on low salinity recovery mechanisms. *J. Phys. Chem. C* **2014**, *118*, 19180−19187.
(37) Rigo, V. A.; Metin, C. O.; Nguyen, Q. P.; Miranda, C. R. Hydrocarbon Adsorption on Carbonate Mineral Surfaces: A First-Principles Study with van der Waals Interactions. *J. Phys. Chem. C* **2012**, *116*, 24538−24548.
(38) Sand, K.; Yang, M.; Makovicky, E.; Cooke, D. J.; Hassenkam, T.; Bechgaard, K.; Stipp, S. Binding of ethanol on calcite: the role of the OH bond and its relevance to biomineralization. *Langmuir* **2010**, *26*, 15239−15247.
(39) Lardge, J. S.; Duffy, D.; Gillan, M. Investigation of the interaction of water with the calcite (10.4) surface using ab initio simulation. *J. Phys. Chem. C* **2009**, *113*, 7207−7212.
(40) Perry, T. D.; Cygan, R. T.; Mitchell, R. Molecular models of a hydrated calcite mineral surface. *Geochim. Cosmochim. Acta* **2007**, *71*, 5876−5887.
(41) De La Pierre, M.; Raiteri, P.; Gale, J. D. Structure and dynamics of water at step edges on the calcite {1014} surface. *Cryst. Growth Des.* **2016**, *16*, 5907−5914.
(42) Cooke, D. J.; Elliott, J. A. Atomistic simulations of calcite nanoparticles and their interaction with water. *J. Chem. Phys.* **2007**, *127*, 104706−104706.
(43) Franco, L.; Castier, M.; Economou, I. G. Anisotropic parallel self-diffusion coefficients near the calcite surface: A molecular dynamics study. *J. Chem. Phys.* **2016**, *145*, 084702.
(44) Cheng, L.; Fenter, P.; Nagy, K.; Schlegel, M.; Sturchio, N. Molecular-scale density oscillations in water adjacent to a mica surface. *Phys. Rev. Lett.* **2001**, *87*, 156103.
(45) Kalinichev, A. G.; Wang, J.; Kirkpatrick, R. J. Molecular dynamics modeling of the structure, dynamics and energetics of mineral-water interfaces: Application to cement materials. *Cem. Concr. Res.* **2007**, *37*, 337−347.
(46) Kenyon, B.; Kleinberg, R.; Straley, C.; Gubelin, G.; Morriss, C. Nuclear magnetic resonance imaging-technology for the 21st century. *Oilfield Rev.* **1995**, *7*, 19−33.
(47) Vincent, B.; Fleury, M.; Santerre, Y.; Brigaud, B. NMR relaxation of neritic carbonates: An integrated petrophysical and petrographical approach. *J. Appl. Geophys.* **2011**, *74*, 38−58.
(48) Sun, T.; Yan, W.; Wang, H.; Golsanami, N.; Zhang, L. Developing a new NMR-based permeability model for fractured carbonate gas reservoirs. *J. Nat. Gas Sci. Eng.* **2016**, *35*, 906−919.
(49) Zhang, F.; Zhang, C.; Rankey, E. *Characterizing petrophysical properties of carbonate rocks using nuclear magnetic resonance and spectral induced polarization*; EGU General Assembly Conference Abstracts; 2016; p 15995.
(50) Rios, E. H.; Figueiredo, I.; Moss, A. K.; Pritchard, T. N.; Glassborow, B. A.; Domingues, A. B. G.; de Vasconcellos Azeredo, R. B. NMR permeability estimators in 'chalk' carbonate rocks obtained under different relaxation times and MICP size scalings. *Geophys. J. Int.* **2016**, *206*, 260−274.
(51) Ozkanlar, A.; Clark, A. E. ChemNetworks: A complex network analysis tool for chemical systems. *J. Comput. Chem.* **2014**, *35*, 495−505.
(52) Plimpton, S. Fast parallel algorithms for short-range molecular dynamics. *J. Comput. Phys.* **1995**, *117*, 1−19.
(53) Markgraf, S. A.; Reeder, R. J. High-temperature structure refinements of calcite and magnesite. *Am. Mineral.* **1985**, *70*, 590−600.
(54) Martínez, L.; Andrade, R.; Birgin, E. G.; Martínez, J. M. PACKMOL: a package for building initial configurations for molecular dynamics simulations. *J. Comput. Chem.* **2009**, *30*, 2157−2164.
(55) Wu, Y.; Tepper, H. L.; Voth, G. A. Flexible simple point-charge water model with improved liquid-state properties. *J. Chem. Phys.* **2006**, *124*, 024503.
(56) Beckers, J.; Lowe, C.; De Leeuw, S. An iterative PPPM method for simulating Coulombic systems on distributed memory parallel computers. *Mol. Simul.* **1998**, *20*, 369−383.

DOI: 10.1021/acs.jpcc.6b12412
J. Phys. Chem. C 2017, 121, 6674−6684

(57) Nosé, S. A unified formulation of the constant temperature molecular dynamics methods. *J. Chem. Phys.* **1984**, *81*, 511−519.
(58) Hoover, W. G. Canonical dynamics: equilibrium phase-space distributions. *Phys. Rev. A: At., Mol., Opt. Phys.* **1985**, *31*, 1695.
(59) Melchionna, S.; Ciccotti, G.; Lee Holian, B. Hoover NPT dynamics for systems varying in shape and size. *Mol. Phys.* **1993**, *78*, 533−544.
(60) Zhu, B.; Xu, X.; Tang, R. Hydration layer structures on calcite facets and their roles in selective adsorptions of biomolecules: A molecular dynamics study. *J. Chem. Phys.* **2013**, *139*, 234705.
(61) Kerisit, S.; Cooke, D. J.; Spagnoli, D.; Parker, S. C. Molecular dynamics simulations of the interactions between water and inorganic solids. *J. Mater. Chem.* **2005**, *15*, 1454−1462.
(62) Allen, M. P.; Tildesley, D. J. *Computer simulation of liquids*; Oxford University Press: 1989.
(63) Krynicki, K.; Green, C. D.; Sawyer, D. W. Pressure and temperature dependence of self-diffusion in water. *Faraday Discuss. Chem. Soc.* **1978**, *66*, 199−208.
(64) Liu, P.; Harder, E.; Berne, B. On the calculation of diffusion coefficients in confined fluids and interfaces with an application to the liquid-vapor interface of water. *J. Phys. Chem. B* **2004**, *108*, 6595−6602.
(65) Karniadakis, G. E.; Beskok, A.; Aluru, N. *Microflows and nanoflows: fundamentals and simulation*; Springer Science & Business Media: 2006; Vol. *29*.
(66) Gordon, R. Correlation functions for molecular motion. *Adv. Magn. Opt. Reson.* **1968**, *3*, 1−42.
(67) Sciortino, F.; Fabbian, L.; Chen, S.-H.; Tartaglia, P. Supercooled water and the kinetic glass transition. II. Collective dynamics. *Phys. Rev. E: Stat. Phys., Plasmas, Fluids, Relat. Interdiscip. Top.* **1997**, *56*, 5397.
(68) Fogarty, A. C.; Coudert, F.-X.; Boutin, A.; Laage, D. Reorientational dynamics of water confined in zeolites. *ChemPhysChem* **2014**, *15*, 521−529.
(69) Romero-Vargas Castrillon, S.; Giovambattista, N.; Aksay, I. A.; Debenedetti, P. G. Effect of surface polarity on the structure and dynamics of water in nanoscale confinement. *J. Phys. Chem. B* **2009**, *113*, 1438−1446.
(70) Halle, B.; Wennerström, H. Interpretation of magnetic resonance data from water nuclei in heterogeneous systems. *J. Chem. Phys.* **1981**, *75*, 1928−1943.
(71) Bloembergen, N.; Purcell, E. M.; Pound, R. V. Relaxation effects in nuclear magnetic resonance absorption. *Phys. Rev.* **1948**, *73*, 679.
(72) Abragam, A. *The principles of nuclear magnetism*; Oxford University Press: 1961.
(73) Delville, A.; Letellier, M. Structure and dynamics of simple liquids in heterogeneous condition: an NMR study of the clay-water interface. *Langmuir* **1995**, *11*, 1361−1367.
(74) Tielrooij, K.; Garcia-Araez, N.; Bonn, M.; Bakker, H. Cooperativity in ion hydration. *Science* **2010**, *328*, 1006−1009.
(75) Calero, C.; Martí, J.; Guàrdia, E. 1H Nuclear Spin Relaxation of Liquid Water from Molecular Dynamics Simulations. *J. Phys. Chem. B* **2015**, *119*, 1966−1973.
(76) Krynicki, K. Proton spin-lattice relaxation in pure water between 0 and 100 C. *Physica* **1966**, *32*, 167−178.
(77) Warne, M.; Allan, N.; Cosgrove, T. Computer simulation of water molecules at kaolinite and silica surfaces. *Phys. Chem. Chem. Phys.* **2000**, *2*, 3663−3668.
(78) Brownstein, K. R.; Tarr, C. Importance of classical diffusion in NMR studies of water in biological cells. *Phys. Rev. A: At., Mol., Opt. Phys.* **1979**, *19*, 2446.
(79) Cohen, M. H.; Mendelson, K. S. Nuclear magnetic relaxation and the internal geometry of sedimentary rocks. *J. Appl. Phys.* **1982**, *53*, 1127−1135.
(80) Schoenfelder, W.; Gläser, H.-R.; Mitreiter, I.; Stallmach, F. Two-dimensional NMR relaxometry study of pore space characteristics of carbonate rocks from a Permian aquifer. *J. Appl. Geophys.* **2008**, *65*, 21−29.
(81) Godefroy, S.; Korb, J.-P.; Fleury, M.; Bryant, R. Surface nuclear magnetic relaxation and dynamics of water and oil in macroporous media. *Phys. Rev. E: Stat. Phys., Plasmas, Fluids, Relat. Interdiscip. Top.* **2001**, *64*, 021605.
(82) Zhao, L.; Ma, K.; Yang, Z. Changes of water hydrogen bond network with different externalities. *Int. J. Mol. Sci.* **2015**, *16*, 8454−8489.
(83) Schön, J. H. *Physical properties of rocks: Fundamentals and principles of petrophysics*; Elsevier: 2015; Vol. *65*.
(84) Luzar, A.; Chandler, D. Effect of environment on hydrogen bond dynamics in liquid water. *Phys. Rev. Lett.* **1996**, *76*, 928.
(85) Soper, A. The radial distribution functions of water and ice from 220 to 673 K and at pressures up to 400 MPa. *Chem. Phys.* **2000**, *258*, 121−137.
(86) Jensen, M. Ø.; Mouritsen, O. G.; Peters, G. H. The hydrophobic effect: molecular dynamics simulations of water confined between extended hydrophobic and hydrophilic surfaces. *J. Chem. Phys.* **2004**, *120*, 9729−9744.
(87) Galicia-Andrés, E.; Dominguez, H.; Pusztai, L.; Pizio, O. Composition dependence of thermodynamic, dynamic and dielectric properties of water-methanol model mixtures. Molecular dynamics simulation results with the OPLS-AA model for methanol. *J. Mol. Liq.* **2015**, *212*, 70−78.
(88) Ozkanlar, A.; Kelley, M. P.; Clark, A. E. Water organization and dynamics on mineral surfaces interrogated by graph theoretical analyses of intermolecular chemical networks. *Minerals* **2014**, *4*, 118−129.
(89) Ohtaki, H.; Radnai, T. Structure and dynamics of hydrated ions. *Chem. Rev.* **1993**, *93*, 1157−1204.
(90) Chen, S.; Teixeira, J. Structure and dynamics of low-temperature water as studied by scattering techniques. *Adv. Chem. Phys.* **1986**, *64*, 1.

DOI: 10.1021/acs.jpcc.6b12412
J. Phys. Chem. C 2017, 121, 6674−6684